

Effect of Number of Walls on Plasmon Behavior in Carbon Nanotubes

M. H. Upton,¹ R. F. Klie,² J. P. Hill,¹ T. Gog,³ D. Casa,³ W. Ku,¹
Y. Zhu,¹ M. Y. Sfeir,¹ J. Misewich,¹ G. Eres,⁴ and D. Lowndes⁴

¹*Condensed Matter Physics and Materials Science Department,
Brookhaven National Laboratory, Upton, New York 11973*

²*Department of Physics, University of Illinois at Chicago, Chicago, IL 60607*

³*CMC-XOR, Advanced Photon Source, Argonne National Laboratory, Argonne, Illinois 60439*

⁴*Condensed Matter Sciences Division, Oak Ridge National Laboratory, Oak Ridge, Tennessee 37830*
(Dated: March 23, 2022)

We investigate the physical parameters controlling the low energy screening in carbon nanotubes via electron energy loss spectroscopy and inelastic x-ray scattering. Two plasmon-like features are observed, one near 9 eV (the so-called π plasmon) and one near 20 eV (the so-called $\pi + \sigma$ plasmon). At large nanotube diameters, the $\pi + \sigma$ plasmon energies are found to depend exclusively on the number of walls and not on the radius or chiral vector. The observed shift indicates a change in the strength of the screening and in the effective interaction at inter-atomic distances, and thus this result suggests a mechanism for tuning the properties of the nanotube.

PACS numbers: 73.22.-f, 73.20.Mf, 78.70.Ck

I. INTRODUCTION

Carbon nanotubes (CNT) have attracted a great deal of interest lately, in part because they may be an ideal material for solar cells. The properties of the exciton are one of the main determinates of the efficiency of a solar cell material. Recent work has demonstrated the profound effect the dielectric screening has on the exciton [1, 2]. These results are particularly tantalizing because, contrary to the conclusions of previous studies [3, 4, 5], it may be possible to tune the dielectric function of CNT by varying the physical parameters of the nanotubes [6].

Further, the possibility of tuning the low energy screening in nanotubes has implications beyond the characteristics of the exciton. CNTs have a variety of unusual properties, including a long electron mean-free-path, quantized electronic and phonon bands and possible Tomonaga-Luttinger liquid behavior [7, 8, 9, 10, 11]. Much of this behavior arises because of the near one-dimensionality of the nanotubes which in turn increases the importance of many-body effects in the system. The influence of many-body effects is controlled in part by the length scale of the low energy interactions. Thus, the possibility of adjusting these interactions through physically accessible parameters is intriguing.

The three key physical parameters affecting the electronic properties of nanotubes are nanotube radius, chiral vector and number of walls: large curvatures in small-radius nanotube walls cause the σ^* and π^* orbitals to hybridize; the chiral vector of nanotubes determines whether the nanotube is metallic or semiconducting; and finally, the number of walls and the nanotube radius both provide quantization conditions for the electron wave functions [7, 12]. However, it is not well understood what effect, if any, these parameters have on the length scale of low energy interactions. The large influence of low energy interactions on the physics and possible applications of nanotubes means it is essential to investigate which pa-

rameters control their length-scale and strength.

In this paper, the $\pi + \sigma$ plasmon energies are studied as a function of nanotube diameter, chirality and number of walls and compared to the $\pi + \sigma$ plasmon energies in bulk graphite. The plasmon energy reflects the low energy screening in the sample. Electron energy loss spectroscopy (EELS) and inelastic x-ray scattering (IXS) are ideal tools for such an investigation, as they both directly probe the dielectric function which determines the screening of the bare interaction [13]. By taking advantage of the complementary strengths of EELS and IXS it is possible to isolate the effects of the three variables and determine that the plasmon frequencies vary only with the number of walls. We show that this shift is not an artifact of the increasing intensity of the surface plasmon with respect to the bulk plasmon, as suggested by previous authors [3, 4, 5, 14]. These results imply that the low energy screening of nanotubes may be tuned simply by changing the number of walls.

II. EXPERIMENT

A. Plasmon energy shift with physical parameters

A large number of EELS studies of plasmons in nanotubes have been previously performed [3, 4, 5, 15, 16]. In particular, the plasmons of single nanotubes [4, 5] and of a randomly oriented, mainly single-walled CNT mat [15, 16] have been studied. Some of these studies have observed an apparent shift in the $\pi + \sigma$ plasmon energy with increasing nanotube diameter and number of walls. However, they did not examine the effects of nanotube diameter and number of walls separately.

Here we demonstrate that the measured shift is not a function of the nanotube diameter or chirality but the number of walls and that it is a real shift in the $\pi + \sigma$ plasmon energy. We begin with a discussion of the EELS

measurements.

The present EELS measurements were performed on a number of isolated double-walled CNTs using an aberration corrected scanning transmission electron microscope (JEOL JEM2200FS), equipped with a Schottky field emission gun operated at 200 keV, an in-column omega energy filter and a CEOS probe corrector. The electron probe size (FWHM) was chosen to be 2 Å to provide sufficient electron beam intensity to study single nanotubes. The collection and convergence angles were 8.9 and 15 mrad respectively. The energy resolution was measured to be 1.0 eV. The beam spot was placed on the center of the tube so that the momentum transfer, which is perpendicular to the beam direction, was tangential to the walls of the nanotube.

The resulting energy loss spectra are shown in figure 1. These data in fact represent an integral over a disk in reciprocal space with a radius of $Q = 5.5\text{\AA}^{-1}$ because of the large acceptance of the detector and the beam convergence angle. Interpreting the spectra quantitatively is further complicated by multiple scattering effects, though based on a comparison of the measured plasmon energies with the plasmon energy dispersions measured with IXS, discussed below, the EELS intensity of figure 1 appears to be dominated by contributions from close to $Q = 0$. For the purposes of the present study, however, the important point is that all the EELS spectra are measured under identical conditions and therefore may be directly compared with each other.

We now discuss effect of the diameter and chirality of the CNT (which changes the curvature of the walls) on the $\pi + \sigma$ plasmon energies. Figure 1 shows measurements from three different, isolated, double-walled CNT with diameters of 3.6, 7.2 and 14.0 nm. These tubes were taken from the same aligned nanotube arrays discussed below. The $\pi + \sigma$ plasmon is clearly visible near 18 eV. Despite the drastically different diameters of the nanotubes, the $\pi + \sigma$ plasmon energies are identical. Although the chirality of the nanotubes was not explicitly checked, it is impossible for nanotubes with different diameters to have the same chiral vectors. Further, it is less than 1% probable that even the two smallest nanotubes would have the same chiral angle. These results therefore explicitly demonstrate, for the first time, that the plasmon energy is independent of nanotube diameter and chirality, for large enough diameters.

In figure 2 a series of EELS scans taken on individual nanotubes with varying number of walls is shown. The $\pi + \sigma$ plasmon energy seems to be dependent on the number of walls of a CNT. The black line in figure 2c-f shows EELS data from the center of nanotubes with 2, 3, 5 and 6 walls respectively. Clearly, the plasmon peak energy shifts with the number of walls. The apparent shift in the $\pi + \sigma$ plasmon energy is therefore exclusively a function of the number of walls and not of the nanotube diameter or chiral vector.

By taking spatially resolved EELS measurements we have been able to show that the energy shift in the $\pi + \sigma$

plasmon is an actual shift in the plasmon energy and not an artifact of the increased amplitude of the surface plasmon relative to a constant energy $\pi + \sigma$ plasmon state as the number of walls decreases, as suggested in previous studies [3, 4, 5]. Figure 2a shows a series of EELS spectra taken at different positions across a double-walled nanotube. This data is qualitatively similar to data in [3]. The spectra from the edge of the tube and the center of the tube are displayed in blue circles. The peak in the edge spectrum has been identified as the surface plasmon state in previous publications [3, 5]. Figure 2b shows an EELS spectrum of graphite. Figure 2c shows the center spectrum from the double-walled nanotube in black, a smoothed graphite spectrum (red), a smoothed edge spectrum (blue) and the sum of the graphite and edge spectrum (purple). It is apparent that the $\pi + \sigma$ plasmon peak in the double-walled nanotube is not a combination of the edge state and the graphite $\pi + \sigma$ plasmon. Figures 2d-f demonstrate this point for nanotubes with 3, 5 and 6 walls. Even for nanotubes with 6 walls, the addition of the graphite and edge spectra give a peak with an energy several eV higher than the measured spectrum. Thus, these EELS spectra show that for a sufficiently low number of walls the measured $\pi + \sigma$ plasmon peak can not be the sum of a surface plasmon peak and a graphite-like $\pi + \sigma$ plasmon peak.

B. Momentum dependence

Having established the existence of a shift of the $\pi + \sigma$ plasmon energy with the number of walls we turn to the momentum dependence of the plasmon shift, and thus the momentum dependence of the change in screening. This momentum dependence can not be measured with EELS. Although, as illustrated above, one of the great strengths of EELS is its ability to study one nanotube at a time, it suffers from limited momentum range due to multiple scattering effects which complicate the data analysis at large momentum transfers. Additionally, in previous studies, orientation information has often been limited by the sample alignment and geometry. To address the momentum dependence of these features therefore, IXS and aligned nanotube samples are utilized.

IXS, like EELS, measures the dynamical structure factor, $S(Q, \omega)$. The advantage of IXS is that the small x-ray scattering cross-section means that there are almost no multiple scattering inelastic events and the interpretation of the data is straightforward, even at high momentum transfers. However, IXS cannot look at individual nanotubes but requires an ensemble of nanotubes. The technique is described in detail elsewhere [13, 17]. The samples studied here were arrays of long, aligned carbon nanotubes [18]. These samples allow for a significant advance over earlier ensemble measurements because they permit measurements of nanotubes in one orientation, rather than a range of orientations. In these experiments, the resolution of the absolute value of Q is set by the in-

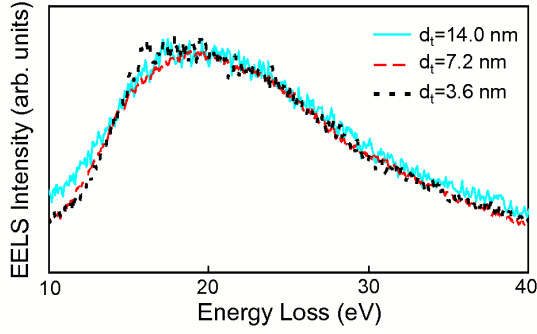


FIG. 1: (color online) EELS spectra from three double walled carbon nanotubes of different diameters. The blue, solid line corresponds to a diameter of 14.0 nm; the black, short-dashed line to a diameter of 7.2 nm and the red, long-dashed line to a diameter of 3.6 nm. The spectra are all taken at the same position in the Brillouin zone and have been normalized to the sample peak intensities. The elastic line has been subtracted off in each case.

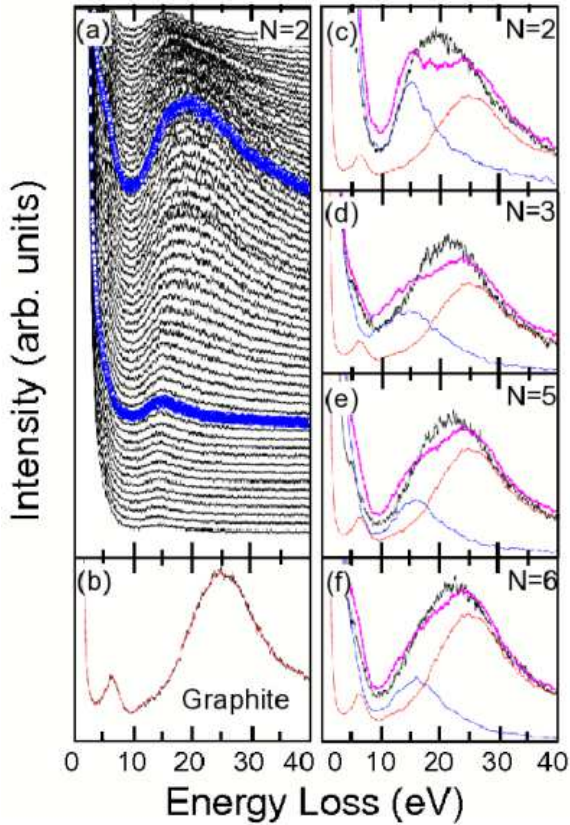


FIG. 2: (color online) (a) EELS spectra from a double-walled nanotube. Different spectra are from different points across the tube. Spectra corresponding to the edge and center of the tube are displayed in blue circles. (b) Raw EELS spectrum from graphite. (c) The center spectrum from a double-walled nanotube (black). The smoothed edge spectrum from this tube is shown in blue and the smoothed graphite spectrum is shown in red. The sum of the edge spectrum and smoothed graphite is shown in purple. (d), (e) and (f) The same as (c) for 3, 5 and 6 walled nanotubes.

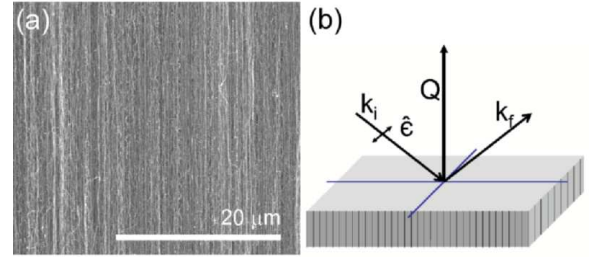


FIG. 3: (color online) (a) Scanning electron microscope picture of an aligned array of multi-walled carbon nanotubes and (b) schematic of the experimental geometry for the x-ray experiments. The axes of the nanotubes are parallel to the direction of momentum transfer, Q .

trinsic resolution of the instrument, 0.056 \AA^{-1} . However, the imperfect alignment of the carbon nanotubes gives rise to uncertainty in the direction of Q . Nevertheless, the combination of IXS and aligned samples allow the excitations to be measured with a larger range of reciprocal space than has been previously possible. We note that this is the first IXS study of carbon nanotubes, though there have been previous IXS studies of the plasmons of graphite [17, 19].

The aligned CNT samples studied here were grown on a Si(001) substrate by chemical vapor deposition [18]. Two types of samples were studied: aligned multi-walled and aligned few-walled carbon nanotube (MW- and FW-CNT) arrays. The tube axes in each case are within 20 degrees of the substrate normal. A scanning electron microprobe picture of one such MWCNT sample is shown in figure 3a. The nanotubes have a relatively low packing fraction (10% – 17%) and are not bunched in ropes, as verified by x-ray transmission and microprobe measurements. Therefore, because the nanotubes are too separated to strongly interact, the results reported here are representative of individual nanotubes and not of a bundle of interacting nanotubes. This is an important point because the environment of a nanotube, for example, a substrate that a nanotube rests on, can change the properties of a nanotube [6, 20].

The physical properties of these nanotube arrays have been characterized by a number of techniques including TEM and Raman spectroscopy. In particular, a series of TEM images show that the MWCNT sample comprises tubes with an average outer diameter of $19 \pm 6 \text{ nm}$ and an average of 14 ± 5 walls, while the nanotubes in the FWCNT sample have an average outer diameter of $5 \pm 2 \text{ nm}$ and 3 ± 2 walls. These parameters are consistent with Raman experiments, which measured breathing modes, characteristic of few-walled NT, in the FWCNT sample but not in the MWCNT sample.

The IXS experiments reported here were performed at beam line 9-ID, CMC-XOR, at the Advanced Photon Source. The overall resolution of the spectrometer was 300 meV (FWHM). The incident photons were polarized, perpendicular to the scattering plane. The polarization

was thus perpendicular to the axis of the nanotubes (figure 3b). Energy scans were performed by varying the incident energy while holding the final energy fixed at 8.9805 keV. In all the data shown here, the direction of the momentum transfer was along the axes of the aligned nanotube samples. Spectra were taken at room temperature.

Representative IXS spectra of the FWCNT sample are shown in figure 4 [21]. Both the $\pi + \sigma$ (~ 20 eV) and π (~ 9 eV) plasmon bands are visible. To extract the plasmon peak positions the spectra were fit with Lorentzians. The quality of the $\pi + \sigma$ fits to some of the data taken at intermediate momentum transfers was improved by fitting a low energy loss shoulder near 22 eV and a small amount of inter-band structure near 28 eV with additional Lorentzians [19]. The addition of these small Lorentzians does not affect the results of this paper, which focuses on the behavior of the large $\pi + \sigma$ plasmon.

We note in passing that carbon nanotube properties are known to be sensitive to the surface adsorption of water and other atmospheric gases [22, 23, 24]. Surface adsorption effects were therefore looked for in the IXS data by outgassing a sample in rough vacuum. Specifically, a sample was heated to 120°C over 90 minutes and then held at 120°C for 3 hours. There was no measurable difference between the spectra before and after this outgassing procedure.

In figure 5a, representative IXS spectra for the FWCNT, MWCNT and HOPG samples are shown. In each case, the data were taken at $Q = 0.79 \text{ \AA}^{-1}$. For the nanotube samples, the momentum transfer was along the axes of the nanotubes and for the graphite sample the momentum transfer was in the plane of the graphite sheets. As was the case in the EELS data, the $\pi + \sigma$ plasmon is observed to shift with the number of walls.

III. DISCUSSION

The most obvious explanation of the $\pi + \sigma$ plasmon shift is that the electron density in the nanotubes decreases as the number of walls decreases. The simplest model of plasmons, the jellium model, predicts the plasmon energy, ω_p , at the center of the Brillouin zone varies with the electron density, n , as $\omega_p \sim \sqrt{n}$ [25]. To explain the observed $\pi + \sigma$ plasmon shift within the context of the jellium model the FWCNT sample would have to have only 76% of the electron density of graphite, an exceptionally large decrease.

A lower electron density may result from a number of causes. The decreased density of graphite in carbon nanotubes may reduce the electron density appreciably. The graphene-graphene distance is larger in nanotubes than in graphite and increases at very small nanotube diameters [26]. However, the predicted difference between the FWCNT and MWCNT densities is less than 1% and the difference between the MWCNT and graphite densities

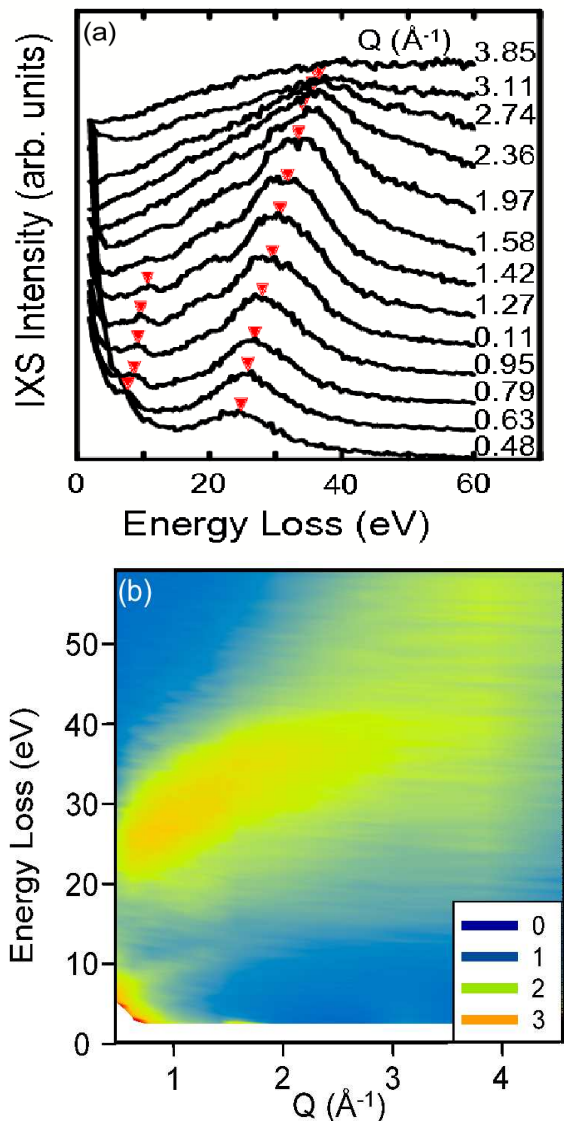


FIG. 4: (color online) (a) Inelastic x-ray scattering spectra from the few-walled carbon nanotube sample. Q is parallel to the nanotubes' axis. The $\pi + \sigma$ plasmon is the large feature between 20 and 40 eV energy loss. The π plasmon is the small peak near 10 eV energy loss. The elastic lines have been omitted in these plots. A red triangle points to the peak positions. Data are offset vertically for clarity. (b) The same data as a contour plot.

is less than 3%.

Another possible cause of the decreased electron density is that the surface tails of the electron wave functions have significantly reduced the electron density in the bulk. When there are only a few walls the surfaces have a greater influence on the nanotube properties than when there are effectively an infinite number of walls. However, to get any reasonable agreement with the data the electron tails of the surface layers need to be excessively large: the integrated intensity of the surface tails

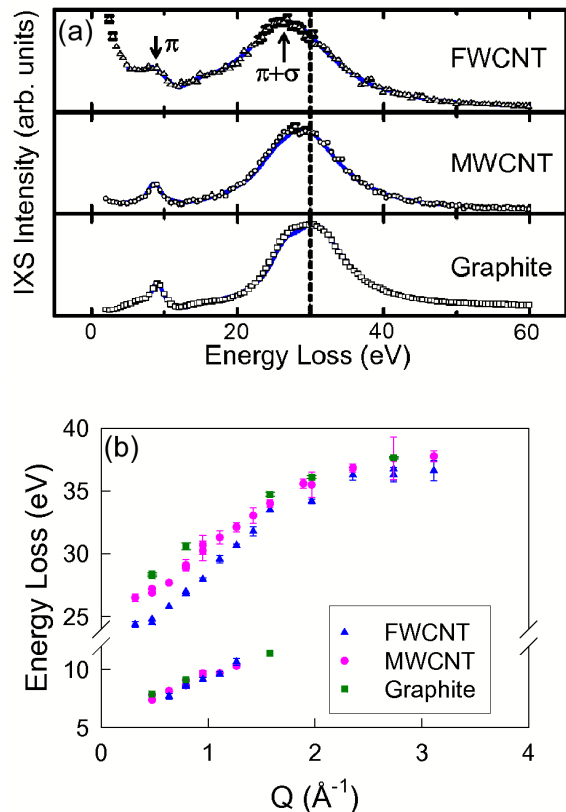


FIG. 5: (color online) (a) Inelastic x-ray scattering spectra from few-walled (top panel), multi-walled carbon nanotube (middle panel) and HOPG (bottom panel). In each case, $Q = 0.79 \text{\AA}^{-1}$ with Q along the nanotubes' axis and in the plane of graphite, respectively. The elastic lines have been omitted in this plot. Note that the tail of the elastic line in the FWCNT spectrum appears unusually large simply because there is less FWCNT material and the inelastic signal is therefore correspondingly smaller than in other cases. (b) Plasmon dispersion for the three samples. The error bars come from the Marquardt least-squares fitting algorithm. When no error bars appear, the error is smaller than the symbol size.

of a surface sheet would be half of the magnitude of the integrated electron intensity of one interior sheet.

Perfect quantitative agreement with a simple model like the jellium model should not be expected. In this case, however, the disagreement is extremely large and one must look for a different explanation.

Instead, we propose that the plasmon energy shift is driven by changes in screening. The momentum dependence of the plasmon energy for the three cases is shown in figure 5b. At large Q , corresponding to small length scales, the difference between graphite, MWCNT and FWCNT $\pi + \sigma$ plasmon energies is small or nonexistent. This makes sense. At these (atomic) length scales, screening effects would be expected to be small, and equal in the three samples. At small and intermediate Q , corresponding to longer length scales, the differences in the plasmon energies are significant, with samples with fewer

walls exhibiting a significantly lower plasmon energy than those with more walls. The energy difference becomes noticeable for $Q \leq 2 \text{\AA}^{-1}$, which corresponds to length scales greater than 3\AA , near the interplanar distance in graphite. As demonstrated above, the $\pi + \sigma$ plasmon energy depends only on the number of walls. The momentum dependence shows this effect is only present for length scales greater than the interplanar spacing. This again makes intuitive sense. At shorter length scales, the presence or absence of neighboring sheets of graphite is not felt, and plasmon energies converge.

The plasmon energy is determined by the zero of the real part of the energy and wave-vector dependent dielectric function, $\epsilon(\mathbf{Q}, \omega)$. From a general understanding of the dielectric constant, our result implies that, at low energies, the magnitude of the dielectric function is smaller in samples with fewer walls. This indicates that the length scale of low energy interactions is longer in FWCNT than in MWCNT, and longer in MWCNT than in graphite. There are a number of consequences of changes in this length scale for the optical properties of the system. For example, it implies that excitons in MWCNT are more likely to dissociate than excitons in FWCNT, because the additional screening in MWCNT decreases the binding energy of excitons.

IV. SUMMARY

We have shown that for diameters larger than 3.6 nm , the $\pi + \sigma$ plasmon energies near $Q = 0$ of CNT samples depend exclusively on the number of walls, and that the shift observed is not an artifact of a relative change in intensity of the surface plasmon. That is, a unique $\pi + \sigma$ plasmon dispersion and a unique $Q = 0$ plasmon energy are associated with a particular number of walls. We infer that the low energy screening, which controls the physical extent of the low energy interactions, is tuned by changing the number of walls in carbon nanotubes.

V. ACKNOWLEDGMENTS

The authors thank C. C. Homes and L. Carr for optical characterization of the samples, A. Stein for electron microprobe pictures of the samples and J. Fink for helpful discussions. Work performed at BNL was supported by US DOE, Division of Materials Science and Engineering, under contract No. DE-AC02-98CH10886 and partially by DOE-CMSN. Use of the Advanced Photon Source was supported by the US DOE, Office of Science, Office of Basic Energy Sciences, under Contract No. W-31-109-Eng-38. Research performed at ORNL was sponsored by the Division of Materials Sciences and Engineering, Office of Basic Energy Sciences, US DOE, under contract DE-AC05-00OR22725.

-
- [1] V. Perebeinos, J. Tersoff, and P. Avouris, Phys. Rev. Lett. **92**, 257402 (2004).
- [2] C. D. Spataru, S. Ismail-Beigi, L. X. Benedict, and S. G. Louie, Phys. Rev. Lett. **92**, 077402 (2004).
- [3] O. Stéphan, M. Kociak, L. Henrard, K. Suenaga, A. Gloter, M. Tencé, and C. Colliex, J. Electron Spectrosc. and Relat. Phenom. **61**, 13936 (2001).
- [4] P. M. Ajayan, S. Iijima, and T. Ichihashi, Phys. Rev. B **47**, 6859 (1993).
- [5] L. A. Bursill, P. A. Stadelmann, J. L. Peng, and S. Praver, Phys. Rev. B **49**, 2882 (1994).
- [6] A. G. Marinopoulos, L. Reining, A. Rubio, and V. Olevano, Phys. Rev. B **69**, 245419 (2004).
- [7] R. Saito, G. Dresselhaus, and M. S. Dresselhaus, *Physical Properties of Carbon Nanotubes* (Imperial College Press, 1988).
- [8] J. Hone, B. Batlogg, Z. Benes, A. T. Johnson, and J. E. Fischer, Science **289**, 1730 (2000).
- [9] B. Gao, A. Komnik, R. Egger, D. C. Glatli, and A. Bachtold, Phys. Rev. Lett. **92**, 216804 (2004).
- [10] R. Tarkiainen, M. Ahlskog, J. Penttilä, L. Roschier, P. Hakonen, M. Paalanen, and E. Sonin, Phys. Rev. B **64**, 195412 (2001).
- [11] M. Bockrath, D. H. Cobden, J. Lu, A. G. Rinzler, R. E. Smalley, L. Balents, and P. L. McEuen, Nature **397**, 598 (1999).
- [12] M. Y. Sfeir, T. Beetz, F. Wang, L. Huang, X. M. H. Huang, M. Huang, J. Hone, S. O'Brien, J. A. Misweich, T. F. Heinz, et al., Science **312**, 554 (2006).
- [13] W. Schülke, *Handbook on Synchrotron Radiation* (Elsevier Science Publishers B. V., 1991), vol. 3, chap. 15, pp. 565–638.
- [14] A. Seepujak, U. Bangert, A. J. Harvey, P. M. F. J. Costa, and M. L. H. Green, Phys. Rev. B **74**, 075402 (2006).
- [15] T. Pichler, M. Knupfer, M. S. Golden, J. Fink, A. Rinzler, and R. E. Smalley, Phys. Rev. Lett. **80**, 4729 (1998).
- [16] M. Kociak, L. Henrard, O. Stéphan, K. Suenaga, and C. Colliex, Phys. Rev. B **61**, 13936 (2000).
- [17] W. Schülke, U. Bonse, H. Nagasawa, A. Kaprolat, and A. Berthold, Phys. Rev. B **38**, 2112 (1988).
- [18] G. Eres, A. A. Puretzky, D. B. Geohegan, and H. Cui, Appl. Phys. Lett. **84**, 1759 (2004).
- [19] N. Hiraoka, H. Ishii, I. Jarrige, and Y. Q. Cai, Phys. Rev. B **72**, 075103 (2005).
- [20] B. J. LeRoy, S. G. Lemay, J. Kong, and C. Dekker, Appl. Phys. Lett. **84**, 4280 (2004).
- [21] The spectra are normalized by incident x-ray intensity and a geometric factor, $1/\cos\theta$, which accounts for variations in the beam footprint on the sample as the scattering angle is varied.
- [22] A. Zahab, L. Spina, P. Poncharal, and C. Marlière, Phys. Rev. B **62**, 10000 (2000).
- [23] P. G. Collins, K. Bradley, M. Ishigami, and A. Zettl, Science **287**, 1801 (2000).
- [24] J. Kong, N. R. Franklin, C. Zhou, M. G. Chapline, S. Peng, K. Cho, and H. Dai, Science **287**, 622 (2000).
- [25] M. P. Marder, *Condensed Matter Physics* (John Wiley & Sons, Inc., 2000).
- [26] C. H. Kiang, M. Endo, P. M. Ajayan, G. Dresselhaus, and M. Dresselhaus, Phys. Rev. Lett. **81**, 1869 (1998).